Int. J. Electrochem. Sci., 13 **(2018)** 12099 – 12117, doi: 10.20964/2018.12.50

International Journal of
ELECTROCHEMICAL
SCIENCE
www.electrochemsci.org

Effects of DC Stray Current on the Polarization Characteristics of X70 Steel

Jun Wang, Zili Li, Chuanping Kong, Ziqing Yang, Jianguo Liu, Gan Cui*

Provincial Key Laboratory of Oil and Gas Storage and Transportation Security, College of Pipeline and Civil Engineering, China University of Petroleum, Qingdao, Shandong, 266580, China
*E-mail: zilimenhuzu@163.com

Received: 21 June 2018 / *Accepted:* 6 August 2018 / *Published:* 5 November 2018

To investigate polarization characteristics of X70 steel at direct current densities in the 50~1200 A/m^2 range under anodic and cathodic interferences, electrochemical method was used to test Tafel polarization curves. The critical current density was 180 A/m^2 and equal or above this value the Tafel polarization curves were linear. By fitting these curves, we obtained polarization resistance R_p, which can be used to characterize the polarization characteristics of X70 steel at DC current. R_p decreased with an increase in the DC current density under both cathodic and anodic interferences. Relational between R_p and DC current density was calculated. As the anodic interference current density increased, corrosion potential of X70 steel shifted positively. Opposite behavior is observed in the case of cathodic interference.

Keywords: DC stray current；X70 steel；corrosion； linear fitting method；polarization resistance

1. INTRODUCTION

Stray current refers to the current flowing through unintended paths [1]. Stray current is typically divided into the direct current (DC), alternating current (AC) and natural telluric current [2]. The DC stray current is mainly produced by DC source such as electrified railways, grounding electrodes of the high-voltage direct current (HVDC) transmission systems and anode beds of cathodic protection system [3-5]. Stray current accelerates corrosion of buried pipelines, compromising their safe operation [6,7]. AC-caused corrosion was studied thoroughly and extensively [8-13], yet, corrosion of pipelines caused by DC is more severe than by AC. It was demonstrated that corrosion rate of steel at 60 Hz AC is about 1% of that at DC current [14]. Pipeline corrosion is especially serious when HVDC transmission systems run with a single electrode due to the thousands of amperes of current leaking into the ground [15]. It is also inconclusive whether X70 steel undergoes regular polarization at DC current.

Several research groups studied corrosion caused by DC stray current. Some research groups conducted numerical simulation using BEASY software studying pipeline corrosion of DC stray current produced by cathodic protection system. [16]. Other researchers showed that corrosion rate of X65 steel increased with the increase of stray DC density; however, at DC density equal to 100 A/m^2, X65 steel passivated and the corrosion rate decreased [17]. It was also found that DC stray current can polarize the pipeline steel X52 at both anodic and cathodic zones [18].

It was reported that when the current leaking into the earth from HVDC transmission system was 1200 A, the current flowing on the buried pipeline was 238.8 A [15]. Such a large current value will be even larger when converted into the current density due to the characteristic of local concentration of stray current corrosion. However, typical current densities studied are less than 200 A/m^2 [17-19], which is far from the real-life circumstances.

Additionally, investigations on the polarization characteristics of carbon steel under cathodic interference have become somewhat limited during the recent years. Majority of the research focuses on anodic interference. Another drawback is that Tafel polarization curves obtained at stray current are generally fitted by the software based on the Tafel extrapolation method [20], but the correctness of the fitting method is not discussed.

In this study, we obtained Tafel polarization curves under the interference of a relatively high DC current density (50~1200 A/m^2) under both anodic and cathodic interference conditions. Our goal was to assess these interferences as close to the actual environment of oil/gas pipelines as possible. We discuss the correctness of the different fitting methods and propose linear fitting method. We also deduced critical current density and polarization resistance R_p from the Tafel polarization curves at DC current. We focused our research on polarization characteristics of the X70 steel (and not on the steel morphology) at DC current to provide guidelines for safe operation of X70 steel pipelines.

2. EXPERIMENTAL

2.1 Electrode and solution

X70 steel 10×10×2 mm in size was used as the working electrode. Its chemical composition is shown in Table 1. The back of the working electrode was welded with a copper wire to ensure the circuit was unblocked. Except for the exposed working 100 mm^2 area, the remaining surface was encapsulated with the epoxy. The working electrode was polished, washed with acetone, rinsed with deionized water and then with anhydrous ethanol and finally dried in a desiccator. All tests were conducted in simulated soil solution composed of 0.03 mol/L NaCl, 0.03 mol/L Na_2SO_4 and 0.01 mol/L $NaHCO_3$.

Table 1. Chemical composition of X70 steel.

composition	C	Si	Mn	P	S	Fe
content / %	0.061	0.24	1.53	0.011	0.0009	balance

2.2 Electrochemical test

A custom-designed experimental setup was used to analyze polarization characteristics of X70 steel at DC current in simulated soil solution at 28℃ (see Figure 1). It consisted of the electrochemical test system, DC current system and isolation system. The electrochemical test system consisted of electrochemical workstation PARSTAT2273 and three-electrode system. The reference electrode was saturated calomel electrode (SCE) and the counter electrode was platinum electrode. Reference electrode was in contact with the solution through the Luggin capillary. The distance from the tip of the Luggin capillary to the working electrode was 1 mm to eliminate the ohmic drop. All tests were conducted at 28 ℃. DC current system consisted of a steady DC power supply SS2323 and two platinum electrodes. The interference was divided into anodic and cathodic ones and the current density was set to 50~1200 A/cm^2. The anodic and cathodic interferences current densities were denoted as I_{ai} and I_{ci}, respectively. Isolation system was a single-phase isolated power transformer GWL-3000VA, connected to the workstation PARSTAT2273 to isolate it from the DC power supply.

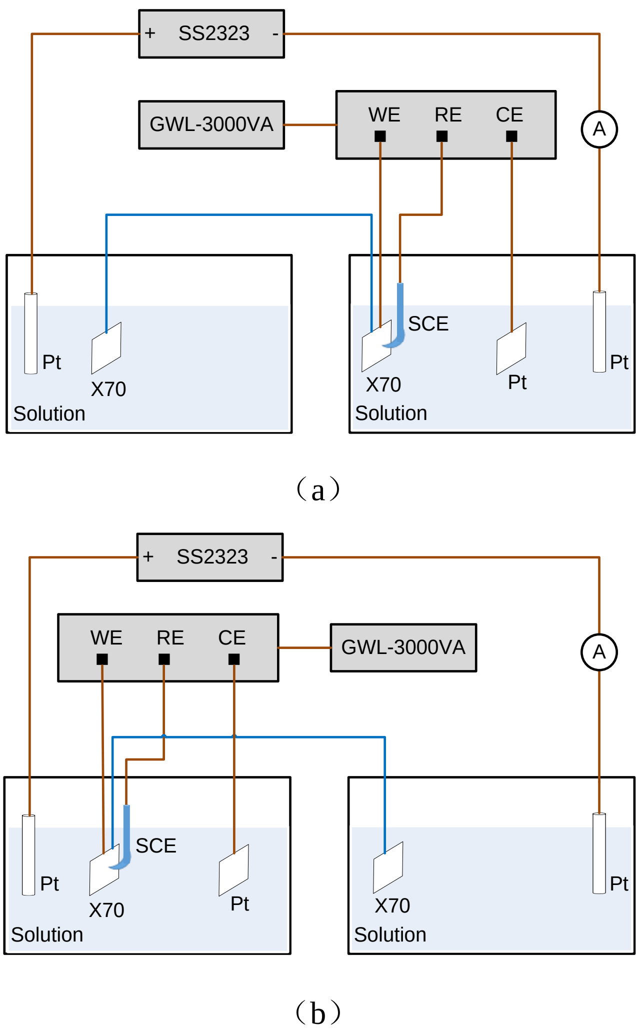

Figure 1. Schematic of the experimental setup for polarization measurements of X70 steel under (a) anodic and (b) cathodic interferences in simulated soil solution at 28℃.

The scanning rate and the range of scanning potential were set to 0.333 mV/s and ± 200 mV (vs. open circuit potential), respectively. Electrochemical tests were repeated three times in parallel experiments at the same current density.

2.3 Conventional methods of data processing

Tafel extrapolation and three-parameter equation fitting methods are the conventional methods of data processing of Tafel polarization curves in the absence of DC current. Tafel extrapolation method is based on the following methodology. Data of Tafel region are selected and then fitted by the PowerSuite software. Through this fitting, corrosion potential (E_{corr}), corrosion current density (I_{corr}) and Tafel slopes (β_a, β_c) are obtained. Three-parameter equation fitting method is based on the data of the Tafel polarization curve. Data are derived and fitted by the three-parameter equation shown below to obtain I_{corr}, β_a and β_c:

$$I = I_{corr}\left[\exp\left(\frac{\Delta E}{\beta_a}\right) - \exp\left(-\frac{\Delta E}{\beta_c}\right)\right] \quad (1)$$

3. RESULTS AND DISCUSSION

3.1 Effect of anodic interference on polarization characteristics

3.1.1 Data processing of Tafel polarization curves at DC current

Figure 2 shows Tafel polarization curves of X70 steel in simulated soil solution at various anodic interference current densities. Tafel extrapolation method [21,22] （method 1）and the three-parameter equation fitting method （method 2） were used to process the data. I_{corr}, β_a and β_c obtained for the X70 steel using different fitting methods under 200~1200 A/m^2 anodic interference are quite different (see Table 2). In order to analyze the sources of these differences, *E*-log*I* polarization curves were replotted as *E*-*I* curves (see Figure 3), which were then linearly fitted. Correlation coefficients (presented in Table 3) showed good linear relationship between *E* and *I* under 200~1200 A/m^2 anodic interference.

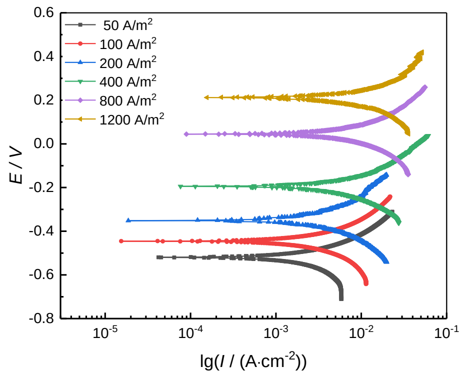

Figure 2. *E*-log*I* polarization curves of X70 steel in simulated soil solution at various anodic interference current densities

Table 2. Electrochemical parameters of X70 steel obtained by different methods under anodic interference.

I_{ai}/（A·m^{-2}）	I_{corr} /（A·cm^{-2}）		β_a/ mV		β_c/ mV	
	Method 1	Method 2	Method 1	Method 2	Method 1	Method 2
50	4.2	4.8	123	146	307	287
100	5.2	6.0	131	161	240	211
200	33.2	22.0	1620	609	1575	372
400	19.6	32.8	452	257	532	440
800	68.7	6.0	1058	126	1915	53
1200	49.8	28.2	698	202	1416	337

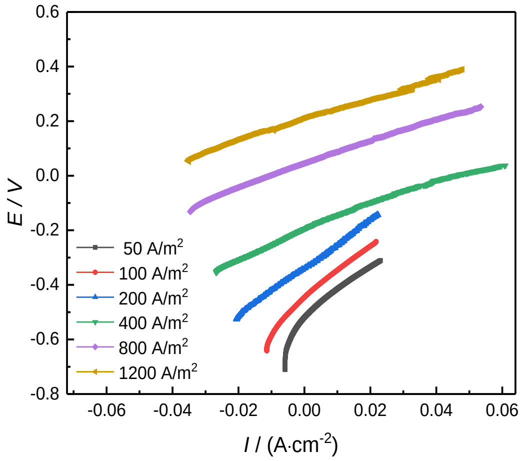

Figure 3. *E-I* polarization curves of X70 steel in simulated soil solution at various cathodic interference current densities

Table 3. Correlation coefficients R^2 obtained from fitting *E-I* curves in Figure 3

I_{ai} / (A·m^{-2})	50	100	200	400	800	1200
R^2	0.747	0.863	0.999	0.999	0.996	0.998

Without DC current, *E-I* polarization curve is fitted using exponential three-parameter equation (such as Equation 1). We expanded Equation 1 using Maclaurin's series of e^x (see Equation 2) at ΔE approaching zero (see Equation 3). Thus, the relationship between ΔE and I is as shown in Equation 4 and it was obtained according to the Equation 3. ΔE is linearly related to I at ΔE approaching zero [23]. However, high-order phase of Maclaurin's series cannot be ignored as ΔE increases. As a result, the *E-I* polarization curves deviate gradually from the straight line forming a non-linear relationship as shown in Figure 4. Thus, linear relationship between E and I implies that it cannot be fitted well using three-parameter equation.

$$e^x = 1 + x + \frac{1}{2!}x^2 + \cdots + \frac{1}{n!}x^n + o\left(x^n\right) \qquad (2)$$

$$I = I_{\mathrm{corr}}\left\{\left[1+\frac{\Delta E}{\beta_{\mathrm{a}}}+o\left(\frac{\Delta E}{\beta_{\mathrm{a}}}\right)\right]-\left[1-\frac{\Delta E}{\beta_{\mathrm{c}}}+o\left(-\frac{\Delta E}{\beta_{\mathrm{c}}}\right)\right]\right\} = I_{\mathrm{corr}}\left[\frac{(\beta_{\mathrm{a}}+\beta_{\mathrm{c}})}{\beta_{\mathrm{a}}\cdot\beta_{\mathrm{c}}}\Delta E + o(\Delta E)\right] \quad (3)$$

$$\Delta E = \frac{\beta_{\mathrm{a}}\cdot\beta_{\mathrm{c}}}{(\beta_{\mathrm{a}}+\beta_{\mathrm{c}})\cdot I_{\mathrm{corr}}} I \quad (4)$$

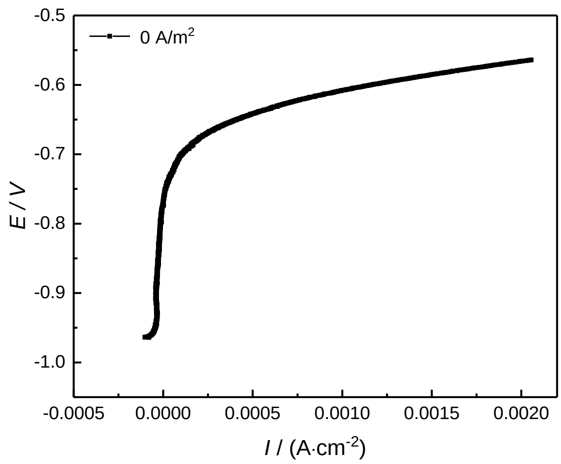

Figure 4. *E-I* polarization curve of X70 steel in simulated soil solution in the absence of DC current.

At large values of DC current density, the surface of the working electrode dissolves and become very rough, distorting corrosion current density obtained from the Tafel region [24]. I_{corr}, β_{a} and β_{c} fitted using Tafel extrapolation method change irregularly with the increase in I_{ai} (see Table 2). Therefore, when the DC current density is very large, Tafel extrapolation method is not recommended.

In summary, the linear relationship exists between E and I at 200~1200 A/m^2 anodic interference. Neither three-parameter equation nor Tafel extrapolation are recommended for fitting of the linear *E-I* curves. Linear fitting method showed good correlation and the slope of the fitted line represents polarization resistance R_{p}. *E-I* polarization curves at 50, 100 A/m^2 were not linear and could be fitted well using Tafel extrapolation method.

3.1.2 Critical current density

E-I polarization curves were linear at 200~1200 A/m^2 anodic interference and non-linear at 50 and 100 A/m^2. Thus, we believe that a critical current density exists in the 100~200 A/m^2 range and the *E-I* polarization curves are linear at this critical current density. To obtain the critical current density, Tafel polarization curves were recorded at 120, 140, 160 and 180 A/m^2 of anodic interference (see Figure 5 and Figure 6). Linear correlation between E and I (see Figure 6) was improving as the current density increased. Slopes of cathodic and anodic polarization curves k_{c} and k_{a}, respectively, were obtained (see Figure 7). k_{c}, k_{a} and m values, where $m=\frac{|k_{\mathrm{c}}-k_{\mathrm{a}}|}{k_{\mathrm{a}}}\times 100\%$, are summarized in Table 4.

The linear correlation between E and I is considered excellent at $m \leq 10\%$. Thus, based on the data from Table 4, the critical current density was 180 A/m^2. If the anodic interference current density was less than 180 A/m^2, it was denoted as "low I_{ai}"; in all other cases it was denoted as "high I_{ai}".

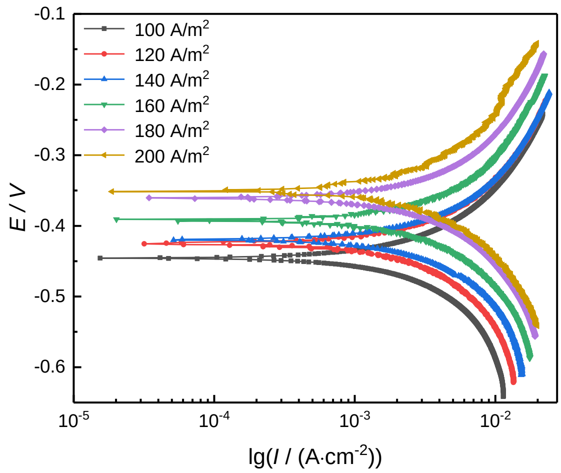

Figure 5. *E*-log*I* polarization curves of X70 steel in simulated soil solution at various anodic interference current densities

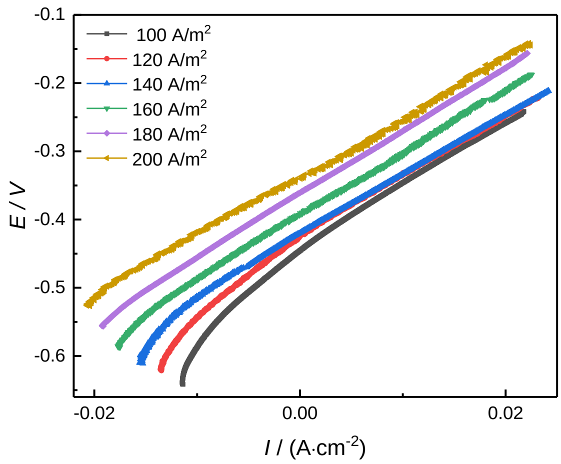

Figure 6. *E-I* polarization curves of X70 steel in simulated soil solution at various anodic interference current densities

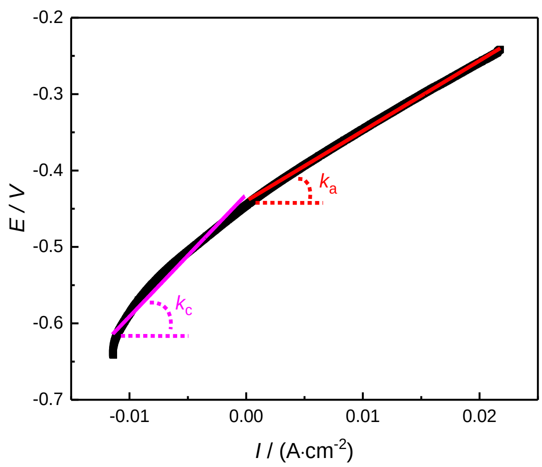

Figure 7. Fitting of the anodic and cathodic polarization curves

Table 4 k_c, k_a and m at various anodic interference current densities

I_{ai} / (A·m^{-2})	k_c	k_a	m / %
50	29.9	8.9	235.6
100	15.9	9.2	73.2
120	13.7	8.7	57.1
140	11.5	8.6	33.1
160	10.7	9.2	15.9
180	9.9	9.2	7.5
200	8.9	9.1	3.0
300	6.9	7.1	2.8

3.1.3 Polarization characteristics at low I_{ai}

Figure 8 shows the E-log$I$ polarization curves of X70 steel at low anodic interference current density. Li et al. [25] found that both anodic and cathodic processes are affected by the current density. When the anodic interference current density increased from 50 to 160 A/m^2 in our experiments, the shape of polarization curves changed, the anodic current density decreased, the cathodic current density increased, and the corrosion potential shifted positively (see Figure 8).

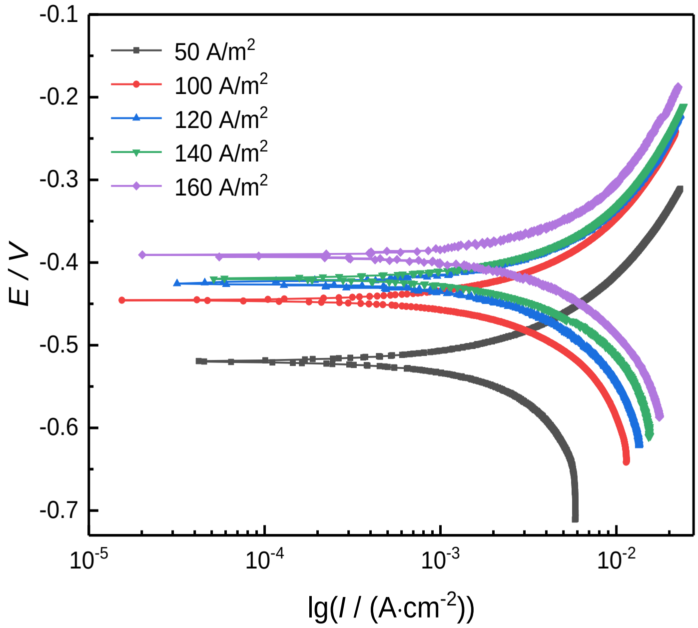

Figure 8. E-log$I$ polarization curves of X70 steel in simulated soil solution at low anodic interference current density.

The E-log$I$ polarization curves at low I_{ai} were fitted by Tafel extrapolation method and the resulting electrochemical parameters, such as E_{corr}, I_{corr}, β_a, β_c and $\beta a/\beta c$, are listed in Table 5.

Table 5. Electrochemical parameters at low I_{ai}.

I_{ai} / (A·m^{-2})	E_{corr} / V	I_{corr} / (A·cm^{-2})	β_a/ mV	β_c/ mV	β_a / β_c
50	-0.52	4.2e-3	123	307	0.40
100	-0.45	5.2 e-3	131	240	0.55
120	-0.43	5.7 e-3	138	211	0.66
140	-0.42	6.1 e-3	141	208	0.68
160	-0.39	6.4 e-3	152	183	0.83

Figure 9 shows the changes of E_{corr} and I_{corr} of X70 steel at various low I_{ai}. As I_{ai} increased, E_{corr} shifted positively and I_{corr} increased. This agrees with the literature results [26-28]. Figure 10 shows changes of β of X70 steel at low I_{ai} values. It was reported in the literature, that Tafel slopes of the anodic and cathodic reactions become more vertical with an increase in the current density, indicating increasing corrosion rate [25]. Zhu et al. [29] found that with an increase in current density, β_a remains unchanged, β_c decreases and the corrosion process shifts from the cathodic control to the mixed control [29]. It was pointed out that polarization curves are different at various current density [30]. In our work, when I_{ai} increased, β_a increased, β_c decreased and the Tafel slope ratio (r = β_a / β_c) increased gradually approaching 1. This indicates that the corrosion process gradually shifted from cathodic control to the mixed cathodic/anodic control.

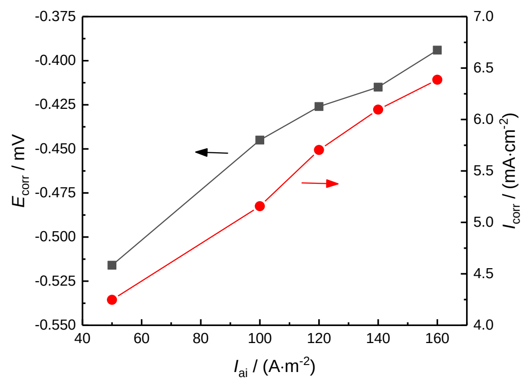

Figure 9. Changes of E_{corr} and I_{corr} of X70 steel at various low I_{ai}

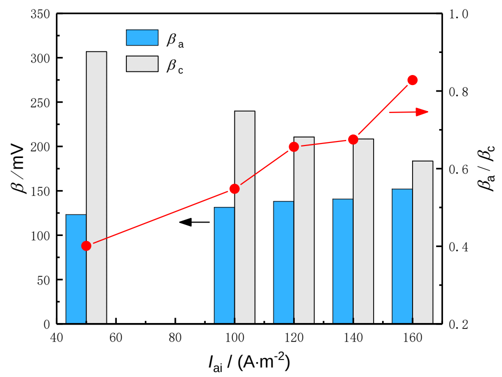

Figure 10. Changes of β of X70 steel at various low I_{ai}

3.1.4 Polarization characteristics at high I_{ai}

Figure 11 shows *E-I* polarization curves of X70 steel at high anodic interference current density. As the current density increased from 180 to 1200 A/m^2, the slope of *E-I* polarization curves became less steep.

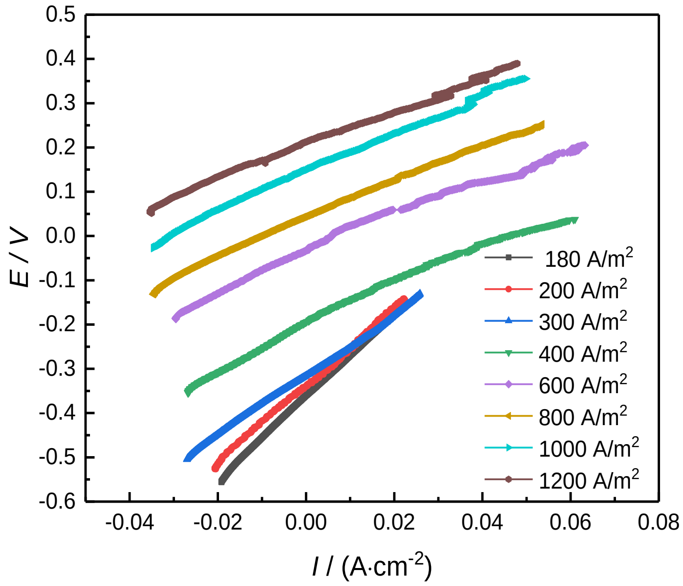

Figure 11. *E-I* polarization curves of X70 steel in simulated soil solution at high anodic interference current density.

E-I polarization curves at high I_{ai} were fitted linearly. All obtained electrochemical parameters (R_p and E_{corr}) are listed in Table 6.

Table 6 Electrochemical parameters at high I_{ai}.

I_{ai} (A·m^{-2})	R_p (Ω•cm^2)	E_{corr} (V)
180	9.33	-0.36
200	8.87	-0.35
300	7.20	-0.29
400	5.34	-0.20
600	4.44	-0.03
800	4.23	0.05
1000	4.19	0.15
1200	3.85	0.21

Figure 12 shows the changes of E_{corr} of X70 steel at various high I_{ai}. As I_{ai} increases, the E_{corr} shifts positively. Figure 13 shows the fitting of R_p at various I_{ai}. The relationship between R_p and I_{ai} can be expressed by the following equation:

$$R_p = 108.28 \times I_{ai}^{-0.481} \qquad (5)$$

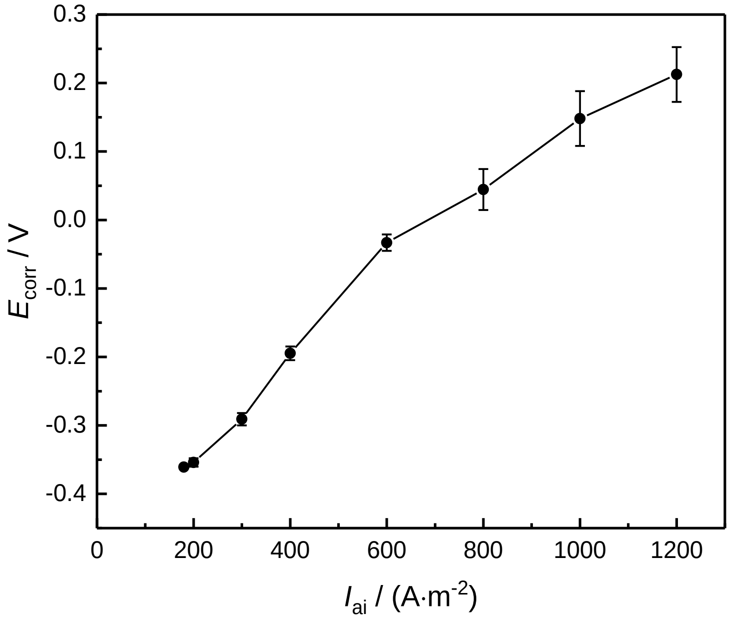

Figure 12. Changes of E_{corr} of X70 steel at various high I_{ai}.

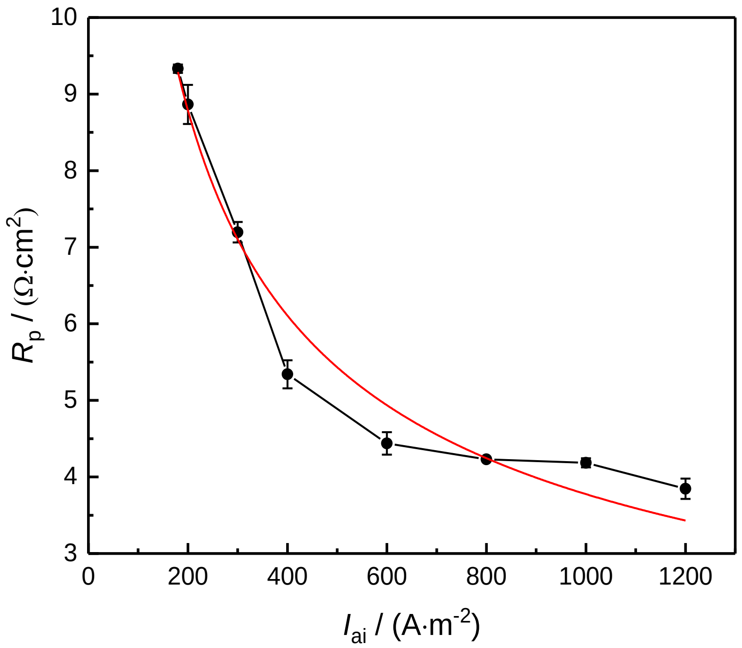

Figure 13. Fitting of R_p of X70 steel at various high I_{ai}.

It was reported that corrosion rate of X80 steel increased gradually as DC current density and stresses increased [27]. Tan et al. [31] found at DC current, the polarization resistance R_p is smaller than without DC current. Figure 13 shows that with the increase in the current density, the polarization resistance R_p decreased. Value of B can be expressed as $B=\left[\left(\frac{df(\Delta E)}{d(\Delta E)}\right)_{\Delta E=0}\right]^{-1}$. For certain corrosion processes, B is a constant. Since $I_{corr}=\frac{B}{R_p}$, the corrosion current density I_{corr} decreases as R_p increases. Thus, R_p could be used to characterize polarization characteristics of X70 steel under anodic interference. The order of the magnitude and the value of R_p reflects severity of the corrosion. The smaller the R_p, the worse the corrosion is.

Corrosion rate of yet another type of steel, Q235 steel, increased as the DC current density increased, but rate of corrosion rise decreased [32]. In our experiments, when current density increased from 180 to 600 A/m^2, R_p decreased sharply, indicating quick acceleration of the X70 steel corrosion. At current density > 600 A/m^2, R_p decreased slowly as the current density increased. At the same time, greenish-gray corrosion products were observed on the surface of the working electrode, which slowed down the severity of the corrosion [33].

3.2 Effect of cathodic interference on polarization characteristics

3.2.1 Critical current density

E-I polarization curves were linearly fitted and the correlation coefficients are reported in Table 7. At 200~1200 A/m^2 cathodic interference was linear, while it was not linear at 50 and 100 A/m^2. Therefore, within 100~200 A/m^2, a critical current density may exist. *E-I* polarization curves were linear at this critical current density. To obtain the critical current density, Tafel polarization curves of X70 steel were measured at 120, 140, 160 and 180 A/m^2 cathodic interference, as shown in Figure 14. Figure 15 shows the linear correlation between E and I, which is improving with the increase in current density. The slopes of cathodic and anodic polarization curves k_c and k_a, respectively, were obtained from fitting. Values of n (which is $n=\frac{|k_a-k_c|}{k_c}\times100\%$), k_c and k_a are summarized in Table 8. Linear correlation between E and I was considered excellent at $n\leq10\%$. Thus, according to Table 8, the critical current density was 180 A/m^2. Finally, the cathodic interference current density below 180 A/m^2 was denoted as "low I_{ci}", and all other densities were denoted as "high I_{ci}".

Table 7 Correlation coefficient R^2 at various cathodic interference current densities.

I_{ci} (A/m^2)	50	100	200	300	400	800	1200
R^2	0.747	0.863	0.999	0.999	0.999	0.996	0.998

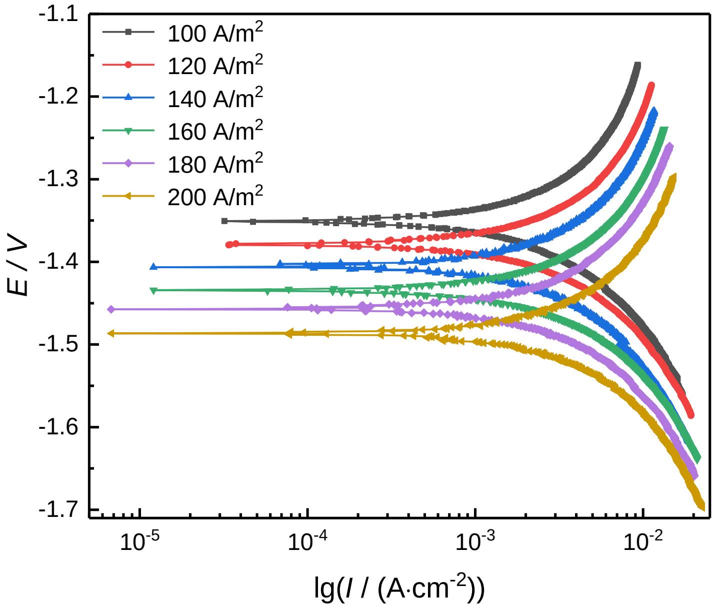

Figure 14. *E*-log*I* polarization curves of X70 steel in simulated soil solution at various cathodic interference current densities.

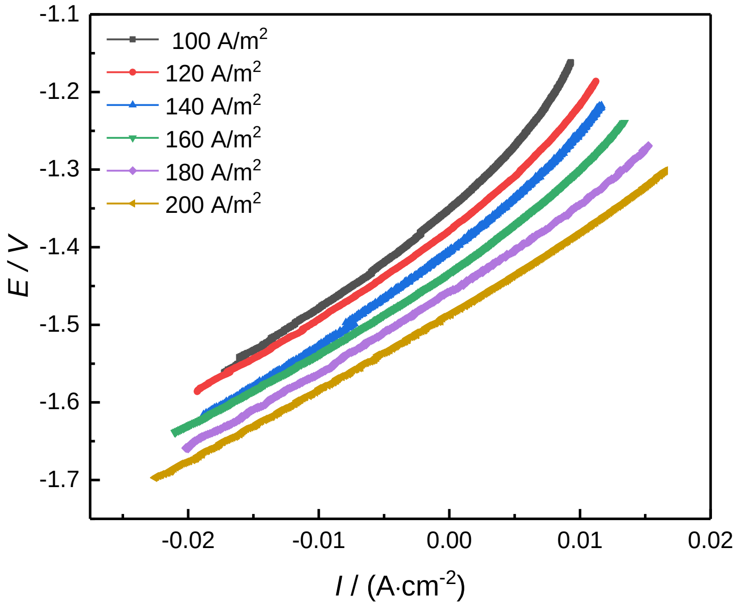

Figure 15. *E*-*I* polarization curves of X70 steel in simulated soil solution at various cathodic interference current densities.

Table 8 k_c, k_a and *m* at various cathodic interference current densities.

I_{ci} (A/m^2)	k_c	k_a	n / %
50	13.7	33.0	140.8
100	11.9	20.1	68.5
120	10.6	16.9	59.9

140	12.0	16.1	33.9
160	11.1	13.4	20.4
180	10.9	12.0	9.8
200	10.4	11.4	9.5
300	9.9	10.7	8.7

3.2.2 Polarization characteristics at low I_{ci}

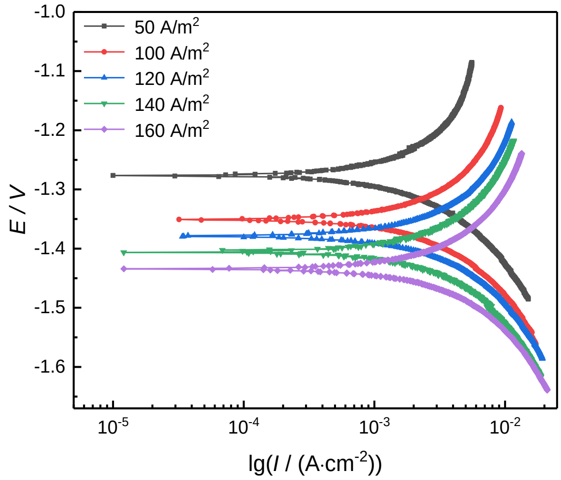

Figure 16. *E*-log*I* polarization curves of X70 steel in simulated soil solution at low cathodic interference current density.

As it can be seen from Figure 16, as the current density increases from 50 to 160 A/m^2, the shape of polarization curves changes, the anodic current density increases, the cathodic current density decreases and the corrosion potential shifts negatively.

The *E*-log*I* polarization curves at low I_{ci} were fitted by Tafel extrapolation method and the obtained electrochemical parameters (E_{corr}, I_{corr}, β_a, β_c and $\beta a/\beta c$) are listed in Table 9.

Table 9. Electrochemical parameters at low I_{ci}.

I_{ci} / (A·m^{-2})	E_{corr} / V	I_{corr} / (A·cm^{-2})	β_a/ mV	β_c/ mV	β_a / β_c
50	-1.28	2.8 e-3	261	122	2.14
100	-1.35	3.6 e-3	199	128	1.56
120	-1.38	4.0 e-3	182	131	1.39
140	-1.41	4.1 e-3	174	131	1.33
160	-1.42	4.5 e-3	172	132	1.30

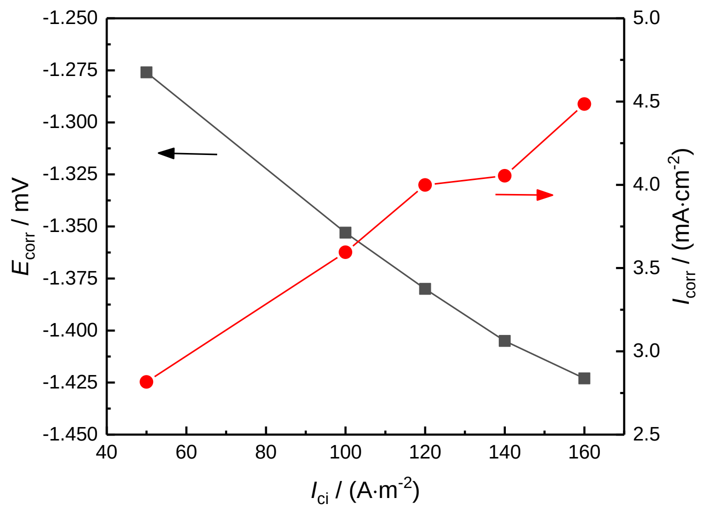

Figure 17. Changes of E_{corr} and I_{corr} of X70 steel at various low I_{ci}.

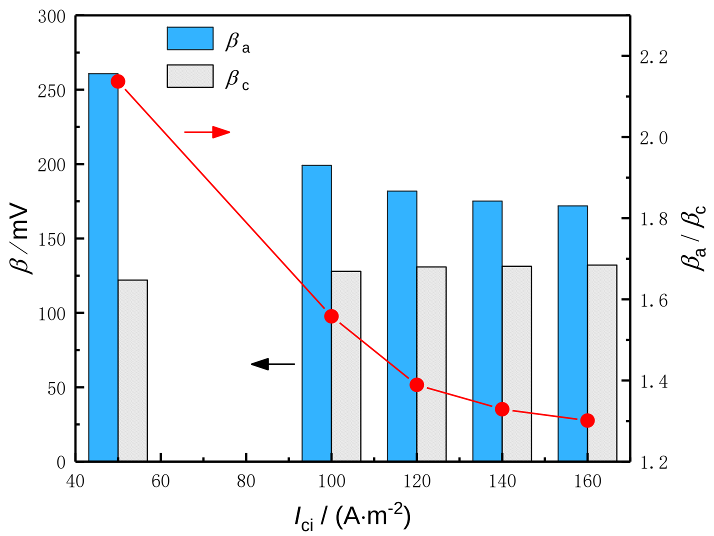

Figure 18. Changes of β of X70 steel at various low I_{ci}.

Figure 17 shows the changes of E_{corr} and I_{corr} of X70 steel at low I_{ci} values. As I_{ci} increases, E_{corr} shifts negatively and I_{corr} increases. Figure 18 shows that as I_{ci} increases, β_a decreases, β_c increases and the Tafel slope ratio (r = β_a / β_c) decreases gradually approaching 1. This indicates that the reaction gradually shifts from anodic control to cathodic and anodic mixed control.

3.2.3 Polarization characteristics at high I_{ci}

Figure 19 shows the *E-I* polarization curves of X70 steel at high cathodic interference current density. As the current density increases from 180 to 1200 A/m^2, the slope of *E-I* curves decrease.

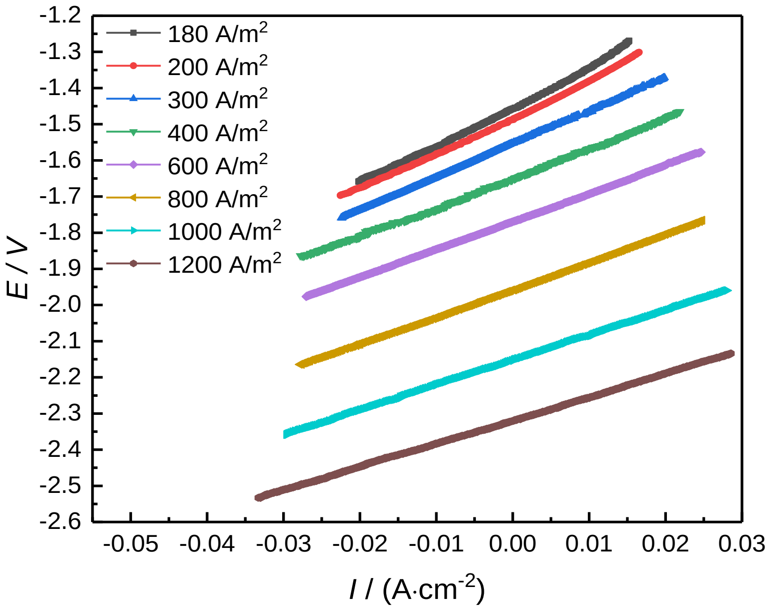

Figure 19. *E-I* polarization curves of X70 steel in simulated soil solution at high cathodic interference current density.

The *E-I* polarization curves at high I_{ci} were fitted linearly and all obtained electrochemical parameters (R_p and E_{corr}) are reported in Table 10.

Table 10 Electrochemical parameters at high I_{ai}.

I_{ci} (A/m^2)	R_p (Ω•cm^2)	E_{corr} (V)
180	11.43	-1.45
200	10.55	-1.49
300	9.98	-1.55
400	8.37	-1.65
600	7.81	-1.77
800	7.68	-1.96
1000	7.40	-2.11
1200	7.16	-2.26

Figure 20 shows the changes of E_{corr} of X70 steel at various high I_{ci}. As I_{ci} increases, E_{corr} shifts negatively. Figure 21 shows the fitting curves of R_p at various I_{ci}. The fitting equation is shown as Equation (6).

$$R_p = 37.954 \times I_{ci}^{-0.24} \tag{6}$$

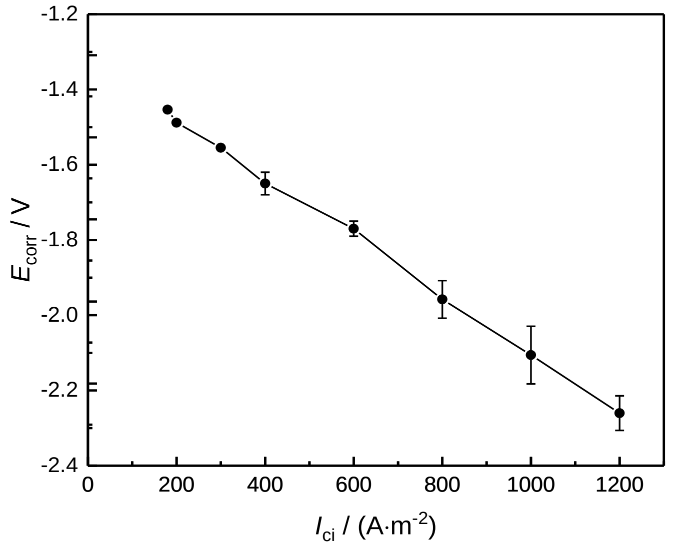

Figure 20. Changes of E_{corr} of X70 steel at various high I_{ci}.

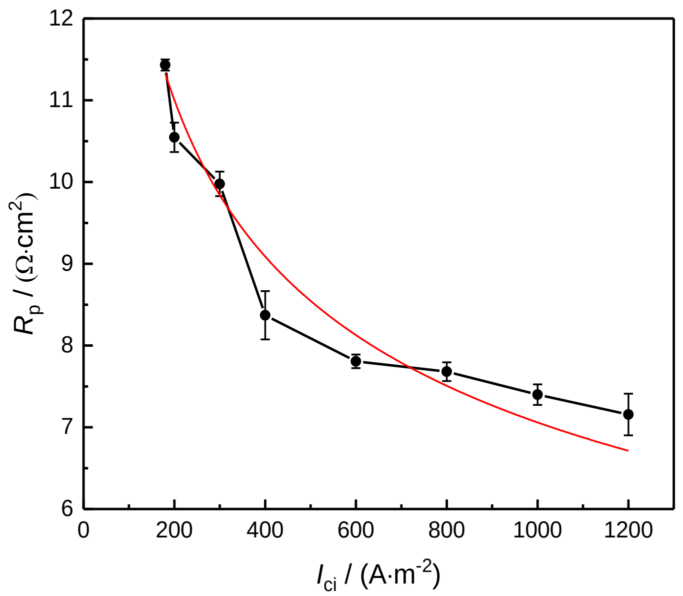

Figure 21. Fitting of R_p of X70 steel at various high I_{ci}.

Figure 21 shows that as the current density increases, the polarization resistance R_p decreases. R_p could be used as a polarization characteristics of X70 steel under cathodic interference. In our study R_p reflected the degree of overprotection. Qian et al. [26] pointed out that the cathodic protection (CP) potential of X52 steel shifted negatively with an increase in DC current density in the cathodic zone. Liu et al. [34] believed that the application of the CP potential should be within a certain range. Excessive negative CP potential may create the "overprotection" possibility, causing hydrogen embrittlement. Zhang et al. [35] found that with the negative shift of the cathodic polarization potential, both the maximum tensile strength and the susceptibility to hydrogen embrittlement increase for the X70 steel. We suggest that the smaller the R_p, the greater the degree of overprotection is and the X70 steel is more likely to be damaged.

4 CONCLUSION

The electrochemical method was used to test and analyze Tafel polarization curves of X70 steel in simulated soil solution at DC current. The following conclusions were reached.

(1) With an increase in the anodic and cathodic interference current densities, corrosion potentials of X70 steel shifted positively and negatively, respectively.

(2) Tafel polarization curves at DC current were linearly fitted. From this fitting, polarization resistance R_p was obtained. The critical current density was 180 A/m^2. At this value, *E-I* polarization curves were very linear.

(3) At DC current density < 180 A/m^2, Tafel extrapolation is the best fitting method. With an increase in the anodic interference current density, the corrosion current density of X70 steel increased and the Tafel slope ratio (r = β_a / β_c) increased slowly approaching 1. This is indicative of the corrosion process gradually shifting from cathodic control to cathodic and anodic mixed control. However, with an increase in the cathodic interference current density, the Tafel slope ratio(r = β_a / β_c) decreased slowly approaching 1. This is indicative of the reaction gradually shifting from anodic control to cathodic and anodic mixed control.

(4) At DC current density equal or above 180 A/m^2, the linear fitting method is the best. Polarization resistance R_p decreased with an increase in the DC current density for both types of interferences. The relational between R_p and DC current density was established. In the case of the anodic interference, R_p reflects the severity of the corrosion: the smaller the R_p, the worse the corrosion was. In the case of cathodic interference, R_p reflects degree of overprotection. The smaller the R_p, the greater the degree of overprotection was and the X70 steel was more likely to be damaged.

References

1. S. Papavinasam, R.W. Revie, *Uhlig's Corrosion Handbook*, Wiley, (2000) New York, USA.
2. B. Gao, L.S. Shen, X.Q. Meng, L.J. Yan, H.C. Han, *Pipeline Technique & Equipment*, 4(2010)41
3. K. Zakowski, *Anti-Corrosion Methods and Materials*, 56(2009)330
4. Y. Wang, Y.G. Yan, C.F. Dong, *Corrosion Science & Protection Technology*, 21(2010)117
5. G. Cui, Z.L. Li, C. Yang, X. Wei, *Corrosion Reviews*, 33(2015)233
6. L.Y. Xu, X. Su, Y.F. Cheng, *Corrosion Science*, 66(2013)263
7. L. Bortels, J. Parlongue, W. Fieltsch, S.M. Segall, *Materials Performance*, 49(2010)32
8. Z. Li, C. Li, H. Qian, J. Li, L. Huang, C. Du, *Materials*, 10(2017)720
9. L.Y. Xu, X. Su, Z.X. Yin, Y.H. Tang, Y.F. Cheng, *Corrosion Science*, 61(2012)215
10. D. Kuang, Y.F. Cheng, *Corrosion Science*, 85(2014)304
11. A.Q. Fu, Y.F. Cheng, *Corrosion Science*, 52(2010)612
12. A.Q. Fu, Y.F. Cheng, *Canadian Metallurgical Quarterly*, 51(2013)81
13. Y. Yang, Z.L. Li, C. Wen, *Acta Metallurgica Sinica*, 49(2013)43

14. D. H. Mcintosh, *IEEE Transactions on Industry Applications*, 18(1982)600
15. J.G. Sun, G.F. Cao, C.C. Han, M.X. Lu, *Corrosion & Protection*, 38(2017)631
16. G. Cui, Z.L. Li, C. Yang, M. Wang, *Petroleum Science*, 13(2016)135
17. C. Yang, G. Cui, Z.L. Li, Y.L. Zhao, C.B. Zhang, *International Journal of Electrochemical Science*, 12(2015)316
18. S. Qian, Y.F. Cheng, *Construction & Building Materials*, 148(2017)675
19. X. Wang, X. Tang, L. Wang, C. Wang, Z. Guo, *International Journal of Electrochemical Science*, 9(2014)4574
20. Y.B. Guo, C. Liu, D.G. Wang and S.H. Liu, *Pet. Sci.*, 12(2015)316
21. E. Mccafferty, *Corrosion Science*, 47(2005)3202
22. M.A. Amin, K.F. Khaled, S.A. Fadl-Allah, *Corrosion Science*, 52(2010)140
23. Y.S. Si, X.W. Yang *Journal of Kunming University of Science & Technology*, 28(2003)164
24. C.N. Cao, *Principles of Electrochemistry of corrosion*, Chemical Industry Press, Beijing, China.
25. Y.C. Li, C. Xu, R.H. Zhang, Q. Liu, X.H. Wang, Y.C. Chen, *International Journal of Electrochemical Science*, 12(2017)1829
26. S. Qian, Y.F. Cheng, *Construction & Building Materials*, 148(2017)675
27. X.H. Wang, X.H. Tang, L.W. Wang, C. Wang, Z.Z. Guo, *International Journal of Electrochemical Science*, 9(2014)4574
28. C. Yang, G. Cui, Z.L. Li, C.B. Zhang, Y.L. Zhao, *Materials Protection*, 49(2016)18
29. M. Zhu, Z.Y. Liu, C.W. Du, X.G. Li, L.Y. Wang, *Journal of Materials Engineering*, 43(2015)85
30. Y. Yang, Z.L. Li, C. Wen, *Acta Metallurgica Sinica*, 49(2013)43
31. Z.H. Tan, Z.P. Zhu, F. Pei, J. Fu, X. Tian, B. Zeng, *Corrosion Science and Protection Technology*, 25(2013)207
32. J.F. Yu, M. Zhang, *Materials Protection*, 48(2015)14
33. L.W. Wang, X.H. Tang, X.H. Wang, J.Y. Liu, C. Wang, R.Y. He, *Corrosion & Protection*, 35 (2014) 218
34. Y. Liu, Y. Li, Q. Li, *Acta Metallurgica Sinica*, 49(2013)1089
35. L. Zhang, M. Du, J.F. Liu, Y. Li, P.L. Liu, *Materials Science & Technology*,19(2011)96